Langmuir

ARTICLE

pubs.acs.org/Langmuir

Controllable Synthesis of Water-Soluble Gold Nanoparticles and Their Applications in Electrocatalysis and Surface-Enhanced Raman Scattering

Yan Qiao, Huanfa Chen, Yiyang Lin, and Jianbin Huang*

Beijing National Laboratory for Molecular Sciences (BNLMS), State Key Laboratory for Structural Chemistry of Unstable and Stable Species, College of Chemistry and Molecular Engineering, Peking University, Beijing 100871, China

Supporting Information

ABSTRACT: We report a facile method to synthesize water-soluble gold nanoparticles (AuNPs) using a biosurfactant sodium cholate as reducing reagents and protective groups in aqueous solution at ambient temperature. The diameters (13−70 nm) of uniform AuNPs can be readily adjusted by changing the initial molar ratio of sodium cholate to chloroauric acid ($HAuCl_4$). Also, the alkaline condition of preparative solution is found to affect the size of as-synthesized AuNPs. This synthetic approach is one-step and "green". The obtained AuNPs exhibit a good electrocatalytic activity toward methanol oxidation. Meanwhile, the AuNPs thin films can serve as an efficient substrate for surface-enhanced Raman scattering (SERS). Furthermore, platinum nanoparticles (PtNPs) are also prepared by reducing sodium tetrachloro platinate hydrate with sodium cholate.

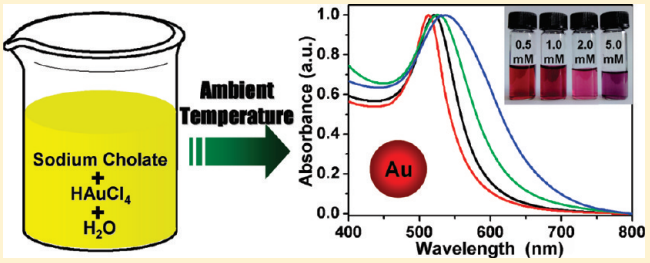

INTRODUCTION

Gold nanoparticles (AuNPs) have stimulated tremendous research interest owing to their fascinating optical, electronic, chemical properties, and promising applications in photoelectric devices, catalysis, biological sensing, and imaging.[1−16] Since the intrinsic characters and relevant applications of AuNPs are closely related with their size, shape, and surface properties, great efforts have been devoted to the controlled synthesis of AuNPs in recent years.[17−31] Preparation of AuNPs usually involves the reduction of metal ions in solutions or at high temperature gaseous environments in the presence of reductive reagents. The high surface energy of these nanosized particles makes them extremely unstable and leads to particle aggregation when AuNPs surface is not well protected or passivated.[32−34] It is therefore highly important to develop new chemical routes to prepare AuNPs that are stable and well dispersible in water. Some of the commonly used methods for AuNPs surface passivation include encapsulation in the water pools of reverse microemulsions[35] and dispersion in polymeric matrixes.[36] The most important route is decorating the AuNPs surface with specific protection ligands.[37] To name a few, Turkevish and Frens pioneered the work of using sodium citrate to reduce auric chloride and stabilize the as-synthesized AuNPs.[38,39] The use of capping reagents such as tiopronin and coenzyme A,[40] 4-(dimethylamino)pyridine (DMAP),[41] and thiol-derivative containing hydrophilic groups[42−46] can also increase the hydrophilicity of AuNPs.

On the other hand, novel environmentally friendly and economically viable methods to synthesize metallic nanomaterials are attracting more and more attention since the topic of "green" chemistry and chemical processes was proposed.[47−53] In this regard, nontoxic chemicals have been introduced as environmentally friendly reducing and capping reagents for the synthesis of noble metal nanoparticles. For example, Wallen and co-workers[54] have successfully synthesized "starched" silver nanoparticles in the size range of 1−8 nm by gently heating an aqueous solution of silver nitrate, soluble starch, and glucose, where glucose served as an environmentally benign reducing reagents, and starch provided stable surface passivation or protection. Sub-10 nm AuNPs have been successfully synthesized by employing β-D-glucose as both a reducing reagent and a capping reagent under controlled pH environments.[55] Mono- and bimetallic nanoparticles have also been prepared in alkaline solution with the reducing and capping ability of β-cyclodextrin.[56]

Inspired by these works, we provide a facile route to synthesize water-soluble AuNPs by using biosurfactant sodium cholate[57] as a reductive reagent and a protective reagent. The cholate-capped AuNPs with narrow size distributions can be conveniently obtained by incubating chloroauric acid with sodium cholate at ambient temperature. The factors such as sodium cholate/$HAuCl_4$ molar ratio and preparative alkaline conditions that affect the size of as-synthesized AuNPs are studied. This approach is considered to be a one-step and "green" process. In addition, the obtained cholate-capped AuNPs are utilized in electrocatalysis

Received: May 22, 2011
Revised: July 13, 2011
Published: July 18, 2011

ACS Publications © 2011 American Chemical Society

dx.doi.org/10.1021/la2019154 | *Langmuir* 2011, 27, 11090–11097

toward the oxidation of methanol and can serve as an efficient substrate for surface-enhanced Raman scattering (SERS). Sodium cholate can be also applied to synthesize platinum nanoparticles (PtNPs).

MATERIALS AND METHODS

Materials. Sodium cholate (Alfa Aesar, 99%), hydrochloroauric acid tetrahydrate ($HAuCl_4 \cdot 4H_2O$, Alfa Aesar, 99.9%), sodium tetrachloroplatinate hydrate ($NaPtCl_4 \cdot H_2O$, Alfa Aesar, 99.95%), and *p*-aminothiophenol (PATP, Alfa Aesar, 96%) were used as received. All the other chemicals were of A.R. Grade of Beijing Chemical Co.

Preparation of Cholate-Capped AuNPs. The synthesis of cholate-capped AuNPs was achieved by the reduction of $HAuCl_4$ with sodium cholate in aqueous solution. In a typical synthesis, 1.5 mL of 100.0 mM sodium cholate solution was maintained at 25 °C for hours. 1.5 mL of 2.0 mM $HAuCl_4$ was added with intensive vortex to give a clear solution. The final concentrations of sodium cholate and $HAuCl_4$ were 50.0 and 1.0 mM, respectively. Then the mixture was kept under static conditions in a thermostat container at 25.0 ± 0.5 °C. If not specific mentioned, the reduction reaction was performed for 5 days. The solution gradually turned into its final appearance (wine red). The intensity of the SPR band was used to monitor the reaction process. The completion of reduction reaction can be indicated by the saturation of UV-vis absorption. Then the AuNPs in solution were collected by centrifugation and washed with deionizeds water for several times. The concentrations of sodium cholate or $HAuCl_4$ were varied to examine their effects on the synthesis of AuNPs. The concentration of NaOH was changed to investigate their effects on AuNPs synthesis.

A similar procedure was carried out to synthesize PtNPs. In a typical synthesis, 1.5 mL of 100.0 mM sodium cholate solution was maintained at 40 °C for hours. 1.5 mL of 10.0 mM $NaPtCl_4$ was added with intensive vortex to give a clear solution. The final concentrations of sodium cholate and $NaPtCl_4$ were 50.0 and 5.0 mM. Then the mixture was kept under static conditions in a thermostat container at 40.0 ± 0.5 °C. If not specific mentioned, the reduction reaction was performed for 3 days. The solution gradually turned into its final appearance (gray black).

Characterization of Sodium Cholate-Capped AuNPs. The cholate-capped AuNPs were characterized by transmission electron microscopy (TEM, FEI Tecnai T20, 200 kV), scanning electron microscopy (SEM, Hitachi S4800, 5 kV), high-resolution TEM (HRTEM, JEM-2100F, 200 kV), X-ray diffraction (XRD, Rigaku Dmax-2000, Ni-filtered Cu Kα radiation), ultraviolet−visible (UV−vis) spectrophotometry (Beijing Purkinje General Instrument Co., Ltd. TU-1810), Fourier transform infrared spectrophotometry (FT-IR, NICOLET iN10 MX, Thermo Scientific), and Zeta PALS Zeta Potential Analyzer (Brookhaven Instruments). For TEM and SEM measurements, the obtained products were dispersed in water and dropped onto a Formvar-covered copper grid and a silicon wafer, respectively, followed by drying in air. For XRD measurements, dry powder of AuNPs was filled into a fillister on clean glass slide. For UV−vis and Zeta Potential measurements, the well-dispersed AuNPs in deioned water were used. For FT-IR, dry powder of AuNPs was examined with microattenuated total reflection (ATR) method.

Dynamic Light Scattering (DLS). DLS was performed with a spectrometer (ALV-5000/E/WIN Multiple Tau Digital Correlator) and a Spectra-Physics 2017 22 mW He/Ne laser (632.8 nm wavelength). The scattering angle was 90°, and the intensity autocorrelation functions were analyzed by using the methods of Contin.

Electrochemical Measurements. A CHI 706 electrochemical workstation (CHI Instrument Co., Austin, TX) with a conventional three-electrode cell was used to perform electrochemical measurements. The working electrode was a glassy carbon electrode with a diameter of 4 mm. A KCl saturated calomel electrode (SCE) was used as the reference electrode and a platinum electrode as the auxiliary electrode. All the electrochemical experiments were conducted at ambient temperature (20 ± 0.5 °C) under N_2 protection. For the preparation of AuNPs-modified GC electrodes (GC), the prepared AuNPs were dispersed in deionized water to obtain a uniform suspension by sonication. Glassy carbon electrodes were first polished with 0.3 and 0.05 μm alumina slurries successively and then washed ultrasonically in distilled water and ethanol for 5 min. The GC electrodes were coated by casting 5 μL of the AuNPs suspension and drying naturally in the air. Finally, 4 μL of 0.05 wt % Nafion solution in alcohol was cast on the surface of the sample and dried naturally in the air.

Raman Measurements. For the preparation of SERS sample, 5 mL of the as-prepared aqueous dispersion containing cholate-capped AuNPs was first condensed to 50 μL by centrifugation, followed by ultrasonic redispersion. The surface-enhanced Raman scattering (SERS) substrate was prepared by dropping the concentrated dispersion onto the 1 × 1 cm^2 Si (111) wafer, which was allowed to dry naturally in air. Then, the Si wafer covered with the AuNPs thin film was immersed into a PATP solution in ethanol (1 mM) for 30 min. After drying in the dark at room temperature, it was rinsed with deionized water and absolute ethanol several times to remove the free PATP molecules and dried in air. For comparison purposes, a Si wafer covered with Au particles was prepared by directly reduction of 10 mM $HAuCl_4$ by 30 mM ascorbic acid. The reaction took place within 30 min. The obtained gold particles applied as the SERS substrate in a similar way. Raman measurements were conducted with a Renishaw System 1000 Raman imaging microscope (Renishaw plc, U.K.) equipped with a 25 mW (632.8 nm) He−Ne laser (model 127-25RP, Spectra-Physics, USA) and a Peltier-cooled CCD detector (576 pixels × 384 pixels). A 50× objective (NA = 0.80) mounted on an Olympus BH-2 microscope was used to focus the laser onto a spot ~1 μm diameter and collect the backscattered light from the sample.

RESULTS AND DISCUSSION

AuNPs Preparation and Characterization. As a representative demonstration, the preparation of AuNPs by reducing 1.0 mM $HAuCl_4$ with 50.0 mM sodium cholate at 25 °C will be discussed in detail. Figures 1a and 1b present typical low- and high-magnification transmission electron microscopy (TEM) images of the cholate-capped AuNPs, which shows uniform gold spheres with a diameter of 20.0 ± 2.0 nm. It is found from TEM images that AuNPs are well-dispersed without any aggregation, indicating the colloidal stability of these dispersions. Dynamic light scattering (DLS) provides a measure for the mean hydrodynamic radius of AuNPs. As Figure 1d shows, the mean hydrodynamic radius is about 18.0 nm, namely, 36.0 nm in diameter, which is relatively bigger than that derived from TEM. This can be rationalized that nanoparticle aggregation may occur during DLS measurement or sample preparation. Different from TEM technique, DLS cannot effectively differentiate the dispersed nanoparticle and aggregated nanoparticles; even a minor fraction of nanoparticle aggregation may result into relatively larger nanoparticle diameter in DLS. In addition, the difference may also originate from different measuring principle of DLS, in which the apparent hydrodynamic diameter is greatly influenced by the ligand shell and surface charge.[58−60] The selected area electron diffraction (SAED) pattern illustrates that AuNPs are polycrystalline and adopt a face-centered cubic (fcc) structure (Figure 1b, inset). The high-resolution TEM (HR-TEM) images shown in Figure 1c exhibit interplanar spacing of 0.235 nm, corresponding to the (111) planes fcc Au.

Energy-dispersive spectroscopy (EDS, Figure 2a) exhibits peaks exclusively attributed to Au besides the Cu and C signals arising from the carbon-covered copper grid. X-ray diffraction (XRD, Figure 2b) pattern shows four sharp reflections characteristic of the (111), (200), (220), and (311) planes of an fcc lattice of Au (JCPDS No. 04-0784). The peak corresponding to the (111) plane is more intense than the other peaks. The intensity ratio of (200) and (111) diffraction peaks is 0.36, which is obviously lower than the conventional value (0.52). This suggests that the (111) plane is the predominant orientation.[61,62]

The UV−vis spectrum of the as-prepared AuNPs is given in Figure 3a, which shows a typical absorption profile with a well-resolved peak. The characteristic surface plasmonic resonance (SPR) band of the 20 nm AuNPs is narrow and located at 521 nm, suggesting a good dispersion and narrow size distribution of AuNPs. Figure 3b shows an image of corresponding AuNPs dispersion in deioned water which is wine red in color. In this work, the intensity of the SPR band is used to monitor the reaction process. The SPR intensity is found to monotonically increase with elongating reaction time and reach a constant value after 5 days, indicating the completion of the reaction (Figure S1). The resultant AuNPs dispersion is remarkably stable and remained unchanged after several months of storage under ambient conditions.

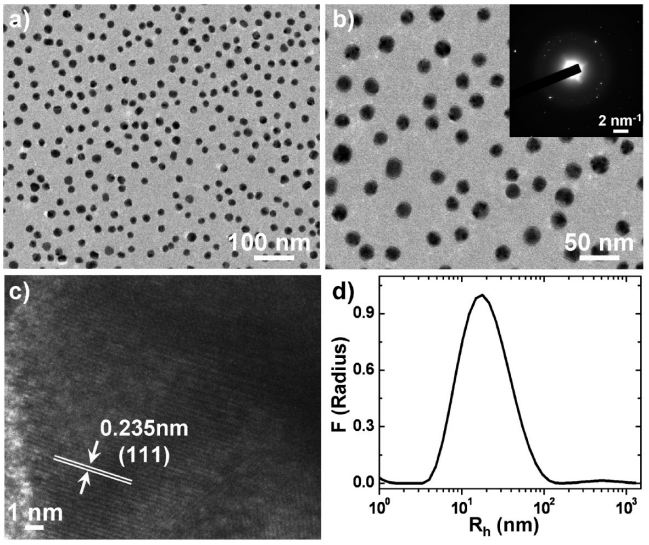

Figure 1. As-prepared AuNPs: (a) low- and (b) high-magnification TEM and (c) HRTEM images. Inset in (b) shows the corresponding ED pattern. (d) DLS analysis.

Tuning the Size of AuNPs. The size variation of AuNPs is found to be realized upon varying the initial molar ratio between sodium cholate and $HAuCl_4$. Figure 4a−c shows the representative TEM images collected from a set of AuNPs dispersions prepared at different sodium cholate/$HAuCl_4$ ratio. Herein, the concentration of sodium cholate is fixed at 50 mM while the initial $HAuCl_4$ concentration increases gradually. As shown in TEM images, the average diameters of nanoparticles are found to increase from 14.4 ± 2.0, to 24.7 ± 4.0, and 46.7 ± 6.0 nm when $HAuCl_4$ concentrations is 0.5, 2.0, and 5.0 mM, respectively. Consistent with this microscopic evidence, DLS results (Figure 5a) also give the nanoparticle diameters of 27.0, 46.9, and 92.0 nm, which further confirm the tendency of AuNPs size increase.

It is well-known that the position and intensity of the SPR band depend largely on the size and aspect ratio of gold nanocrystals.[26,27,30,62] The UV−vis absorption spectra of AuNPs in Figure 5b shows that the SPR band of these AuNPs dispersions red-shifts from 513, 526, to 531 nm with increasing the initial $HAuCl_4$ concentrations from of 0.5, 2.0, to 5.0 mM. The insert photo of AuNPs dispersions' macroscopic appearance shows the color changes gradually from red to purple. This is in accordance with TEM and DLS results, suggesting the particle size increases with decreasing sodium cholate/$HAuCl_4$ ratio.

In an alternative way, the sodium cholate/$HAuCl_4$ ratio can be changed by increasing sodium cholate concentration while $HAuCl_4$ concentration is kept at 1.0 mM. As Figures S2 and S3a show, the diameter of AuNPs decrease from 25.2 ± 2.0, 16.6 ± 2.0, and 13.4 ± 2.0 nm, when sodium cholate concentration increase from 25, 100, to 150 mM, respectively. DLS results (Figure S3b) give the nanoparticle diameters of 48.4, 28.4, and 21.8 nm. The trend is in agreement with the TEM images and further confirms the AuNPs size decrease. The size variation of AuNPs is accompanied by blue-shift in UV−vis spectra (Figure S3b). Meanwhile, the appearances of the AuNPs dispersions

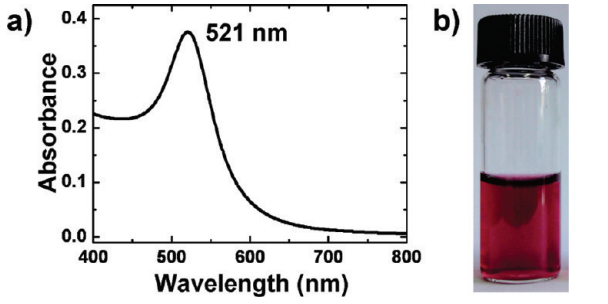

Figure 3. (a) UV−vis spectrum and (b) macroscopic appearance of the as-prepared AuNPs.

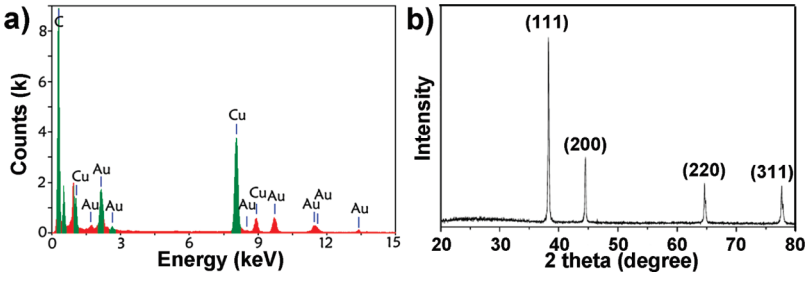

Figure 2. Componential characterization of cholate-capped AuNPs: (a) EDS spectrum and (b) XRD pattern.

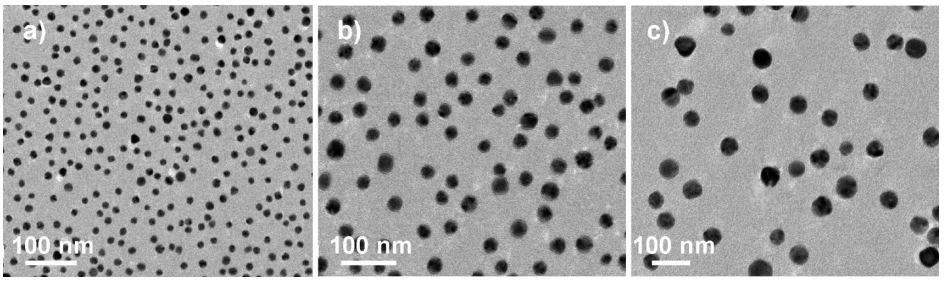

Figure 4. TEM images of AuNPs synthesized at various initial concentration of $HAuCl_4$: (a) 0.5, (b) 2.0, and (c) 5.0 mM. The concentration of sodium cholate is set as 50 mM.

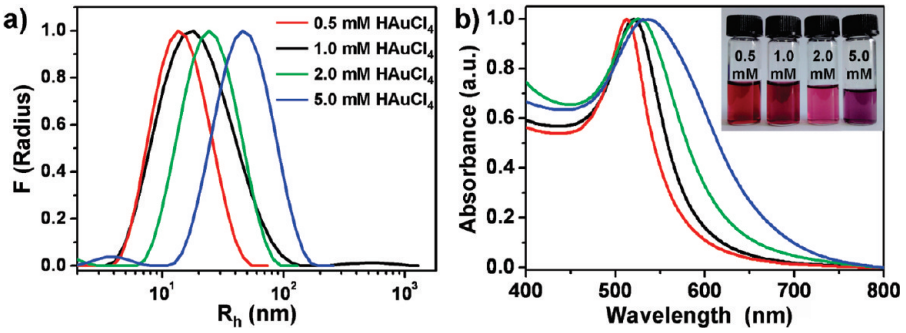

Figure 5. AuNPs obtained at various initial concentration of $HAuCl_4$: (a) DLS analysis; (b) UV−vis spectra. Inset in (b) shows the macroscopic appearance of the AuNPs. The concentration of sodium cholate is set as 50 mM.

Scheme 1. Possible Nucleation−Growth Mechanism of AuNPs Formation

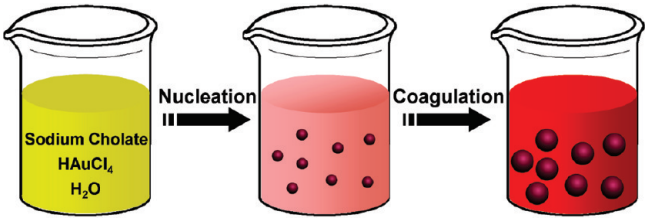

change from purple to red (Figure S3b insert). These results clearly demonstrate this approach can enable facile preparation of AuNPs over a broad size range (13−50 nm), where effective control of nanoparticle size is achieved by varying sodium cholate/$HAuCl_4$ ratio.

AuNPs Growth Mechanism. Because there are only three starting materials, namely, sodium cholate, $HAuCl_4$, and water, it is believed that sodium cholate serves as both reducing reagents and protecting groups in the synthesis of AuNPs. In the literature, the hydroxyl groups often act as the reducing species to reduce Au(III) into metallic Au and can be simultaneously oxidized into carboxylic groups. The oxidation product of cholate bearing negative charge would provide a more efficient capping on the surface of AuNPs due to the Au−COO^- interaction. The capping of cholate on the surface of AuNPs is evident from the Fourier transform infrared (FT-IR) spectra (Figure S4). All the absorption bands of pure sodium cholate (Figure S4a) appear in the spectrum of the cholate-capped AuNPs (Figure S4b), confirming the presence of cholate as an essential component of the as-prepared AuNPs. The zeta potential of the as-prepared dispersion of 20 nm AuNPs was measured to be −23.9 mV, which also indicated that cholate may serve as the capping reagents to provide both steric and electrostatic stabilization for AuNPs.

The nucleation−growth mechanism is illustrated in Scheme 1, which involves three steps: (1) Sodium cholate and $HAuCl_4$ are dispersed in water. (2) Au(III) species are reduced into metallic Au by cholate and AuNPs are formed through a fast nucleation process. Owing to the interaction between AuNPs and carboxyl groups, the cholate molecules will cap on the surface of AuNPs. With the protection of cholate, the Au nucleus aggregation is prevented and the growth of AuNPs is controlled. (3) A coagulation stage which is diffusion-controlled is followed. The data available herein seem to be consistent with the nucleation−growth mechanism of classic citrate reduction route, as demonstrated by the literature.[38,39,63,64] Under this explanation framework, the effect of sodium cholate/$HAuCl_4$ ratio on AuNPs size can be rationalized. In our experiment, the nucleation rate of AuNPs is thought to increase when the concentration of sodium cholate increases (namely, sodium cholate/$HAuCl_4$ ratio increases). On the other hand, a higher sodium cholate concentration means more effective capping of cholate molecules as a stabilization reagent on the particle surface to prevent the particle growth, resulting in smaller Au nanoparticles. After this initial fast nucleation, the number of nanocrystals should keep constant in the following diffusion-controlled growth. Therefore, the final size of the AuNPs should decrease as the concentration of sodium citrate increased, provided that the precursor concentration is fixed.

Alkaline Condition. To reveal the effect of alkaline conditions on the morphology of as-prepared AuNPs, $HAuCl_4$ was reduced by sodium cholate in the presence of different amounts of sodium

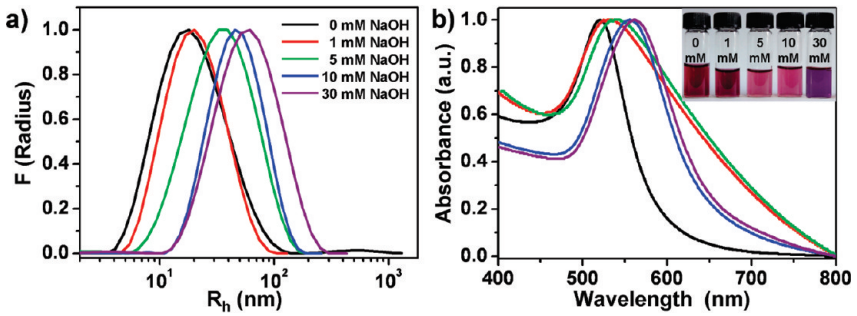

Figure 6. Cholate-capped AuNPs obtained at various concentration of $HAuCl_4$: (a) DLS analysis; (b) UV−vis spectra. Inset in (b) shows the macroscopic appearance of the AuNPs.

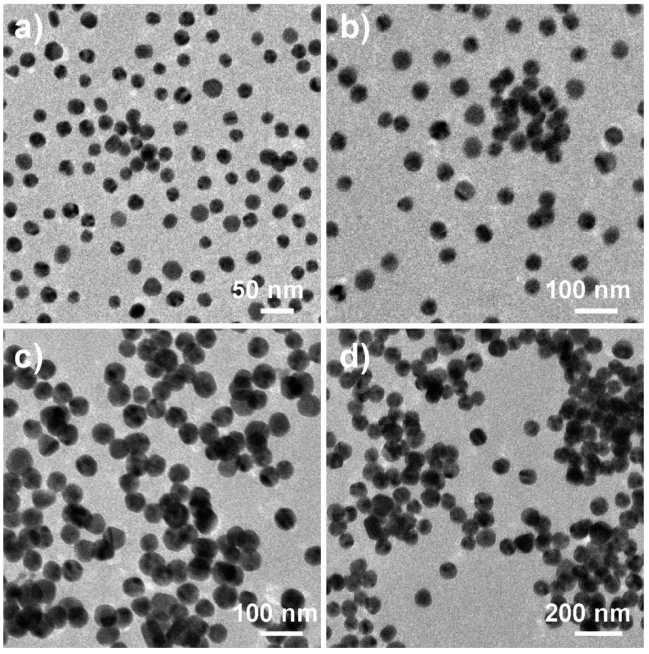

Figure 7. TEM images cholate-capped AuNPs obtained at various concentration of NaOH: (a) 1.0, (b) 5.0, (c) 10.0, and (d) 30.0 mM.

hydroxide. As shown in DLS curves (Figure 6a), the as-obtained AuNPs diameters are 36.0, 40.3, 78.2, 90.6, and 122.4 nm when NaOH concentration is 0.0, 1.0, 5.0, 10.0, and 30.0 mM, respectively. This means the size of AuNPs increases gradually with the increase of NaOH concentration, which is accompanied by the red shift in UV−vis spectra (Figure 6b). Meanwhile, the appearance of the AuNPs solution changes from red to purple (Figure 6b, inset). Collected from TEM images (Figure 7), the diameter of AuNPs is 22.1 ± 2.0, 43.4 ± 4.0, 50.4 ± 6.0, and 68.2 ± 8.0 nm, respectively, when NaOH concentration is 0.0, 1.0, 5.0, 10.0, and 30.0 mM. This confirms that AuNPs become larger at higher alkaline conditions, which is in agreement with DLS result. The result can be explained based on the facts that deprotonation of hydroxyl group can be facilitated at high alkaline conditions, causing the enhancement of reduction ability of hydroxyl group.[56,65] As a result, gold nucleation reaction is accelerated at higher alkaline conditions and larger AuNPs are formed. On the other hand, it is interesting to find that AuNPs tend to aggregate more seriously as the NaOH concentration increases (Figure 7c,d). This is because the larger particle size means larger interparticle van der Waals attraction and the higher salt concentration which may screen the interparticle electrostatic repulsion.

Electrocatalytic Activity of AuNPs. In recent years, electrooxidation of methanol has been commonly used to evaluate the catalytic activity of gold nanomaterials.[66−68] A great advantage of Au as the catalyst toward methanol oxidation is that poisoning intermediates are not formed, although Au is usually considered as a poor catalyst to the reaction.[69,70] It is reported that the catalytic property of AuNPs largely depends on their size and shape.[67,71−73] Accordingly, the AuNPs obtained are deposited onto the commercial GC electrode to prepare AuNPs-modified GC electrodes (denoted as AuNPs electrodes), and their electrocatalytic activity toward the oxidation of methanol is investigated by measuring their cyclic voltammograms (CVs) in KOH solutions. The surface area of the AuNPs electrode is calculated to be 0.0243 cm^2 from the charge consumed during the reduction of surface oxides using the reported value of 400 $\mu C/cm^2$ for a clean Au electrode.[74] This method is a standard electrochemical method frequently used for determining the real surface area of gold, and it has been shown that the value calculated from this method is close to those obtained by methods using redox probes.[72] Thereafter, the measured current is normalized with the surface area to obtain the current density.

For comparison, the electrocatalytic activity of commercial polycrystalline Au electrodes (abbreviated as poly-Au electrodes) is first measured in KOH solution. Figure 8a displays the typical CV images recorded of poly-Au electrode in 0.1 M KOH solutions with and without 2.0 M CH_3OH. In the absence of methanol, the poly-Au electrode shows a broad oxidation wave at about 0.39 V and a relatively sharp reduction wave at about 0.079 V. According to the literature, the oxidation wave could be ascribed to the formation of gold surface oxides, and the reduction wave could be attributed to the subsequent removal of the oxides.[65] When methanol is added, a large anodic wave at 0.243 V is observed for the catalytic oxidation of methanol at the poly-Au electrode, which may be ascribed to the oxidation of methanol to formate via a four-electron-transfer reaction,[69,75] indicating an electrocatalytic activity for the poly-Au. During the negative-going potential sweep, the cathodic peak is at about 0.154 V, corresponding to the reduction of surface oxide.

Furthermore, typical CV images of the AuNPs electrode in 0.1 M KOH solutions with and without 2.0 M CH_3OH are presented in Figure 8b. In the absence of methanol, the AuNPs electrode shows a CV curve quite similar to that of the poly-Au electrode (i.e., a broad oxidation wave at about 0.36 V and a relatively sharp reduction wave at about 0.096 V). When methanol is added, however, the AuNPs electrode shows an oxidation peak at

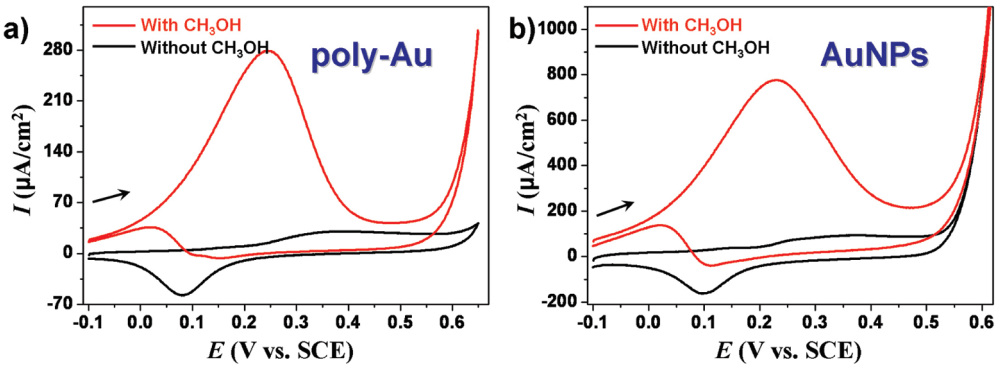

Figure 8. CVs of (a) poly-Au electrode and (b) AuNPs electrode in 0.1 M KOH solutions without CH_3OH or with 2.0 M CH_3OH. Scan rate was 10 mV s^{-1}.

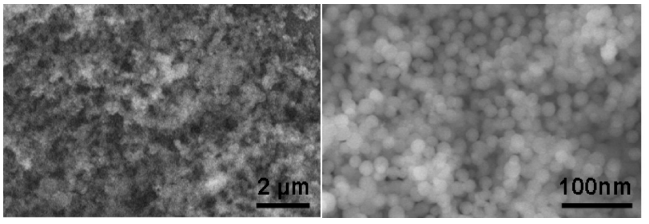

Figure 9. SEM images of cholate-capped 20 nm AuNPs thin film.

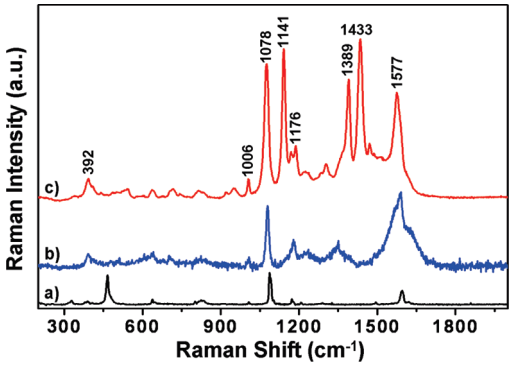

Figure 10. Raman spectrum of (a) solid PATP and SERS spectra of PATP molecules adsorbed on different substrates: (b) gold particles; (c) thin film of 20 nm AuNPs.

0.231 V, which is 12 mV more negative than the oxidation peak potential for the poly-Au electrode (0.243 V). During the negative-going potential sweep, the cathodic peak of AuNPs electrode at about 0.111 V is 43 mV more negative than the reduction peak potential for the poly-Au electrode (0.154 V). Moreover, the current density calculated for methanol oxidation at the AuNPs electrode (780 $\mu A/cm^2$) is 2.78 times that at the poly-Au electrode (281 $\mu A/cm^2$). These results indicate that the AuNPs electrode has higher electrocatalytic activity than poly-Au electrode toward methanol oxidation. The increase in surface area of AuNPs could considerably contribute to their higher electrocatalytic activity as compared to poly-Au.

SERS Activity of AuNPs. It is well-known that gold nanomaterials with good SERS effects have potential applications in identification and biological arrays. Si wafer with thin film of obtained cholate-capped AuNPs can be further used as a SERS substrate. Figure 9 shows typical SEM images of the thin film,

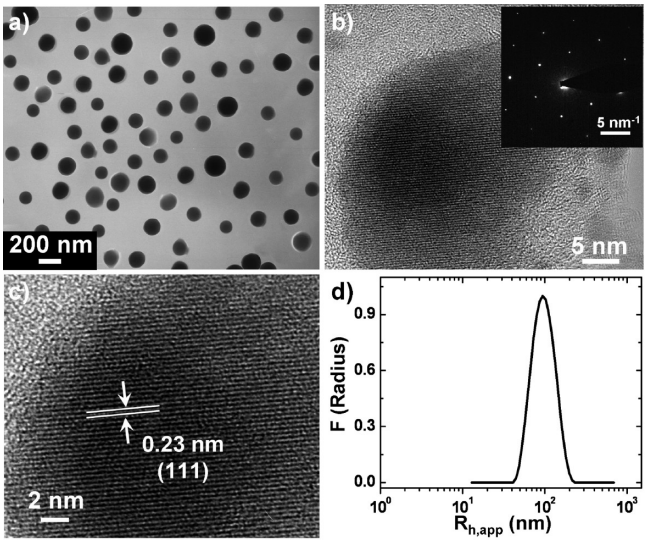

Figure 11. Cholate-capped PtNPs: (a) TEM and (b) low- and (c) high-magnification HRTEM images. Inset in (b) shows the corresponding ED pattern. (d) DLS analysis.

which suggest that the large-area thin film was very smooth and consisted of nearly monodisperse AuNPs with a size of 20 nm. The SERS sensitivity of this thin film is investigated using *p*-aminothiophenol (PATP), which is an important probe molecule in SERS.[76,77] For comparison purposes, gold particles >300 nm in diameter, which are prepared with $HAuCl_4$ directly reduced by ascorbic acid and deposited on the Si wafer, are used as a reference SERS substrate. The Raman spectra of PATP solid and the PATP molecules adsorbed on the two SERS substrates excited with the 633 nm laser line are presented in Figure 10. Compared with Raman spectrum of solid PATP shown in Figure 10a, the Raman shift is changed and the Raman intensity is enhanced in the SERS spectra on the two Au substrates, suggesting that thiol groups in PATP contact with gold surface.[78,79] As shown in Figure 10c, the SERS spectrum of the PATP molecules adsorbed on the cholate-capped AuNPs substrates exhibits the bands at 1577 and 1078 cm^{-1} attributed to a_1 modes (in-plane, in-phase modes), and the bands at 1433, 1389, 1176, 1141, and 1006 cm^{-1} assigned to b_2 modes (in-plane, out-of-phase modes). Generally, the a_1 modes of PATP are predominantly enhanced through the electromagnetic (EM) effect,[80] whereas the b_2 modes are predominantly enhanced through the chemical or

dx.doi.org/10.1021/la2019154 |*Langmuir* 2011, 27, 11090–11097

charge-transfer (CT) effect of metal to the adsorbed molecules, which demonstrates that the PATP molecules make contact with the gold surface by forming a strong Au−S bond.[81] Obviously, the SERS intensity on a cholate-capped AuNPs substrate gains remarkably larger enhancement than that on a gold particles substrate. Particularly, the SERS intensities of the b_2 modes peaks at 1433, 1389, and 1141 cm^{-1} for the cholate-capped AuNPs substrate gain considerably larger enhancement than those for a gold particles substrate. It has been proposed that the enhancement of the Raman intensity of the PATP molecules is largely dependent on the well-crystallized nature of cholate-capped AuNPs and the uniformity of AuNPs thin film, which can be attributed to the improvement of scattering efficiency. This result suggests that the cholate-capped AuNPs thin film could be used as an active SERS substrate.

Preparation and Characterization of Platinum Nanoparticles. Furthermore, it is also found that sodium cholate can be used to synthesize platinum nanoparticles (PtNPs). The reduction of 5.0 mM $NaPtCl_4$ with 50.0 mM sodium cholate at 40 °C will be discussed in detail. Figure 11a presents typical TEM images of PtNPs, which shows that PtNPs are uniform spherical particles with a diameter of 155 ± 17 nm. No significant PtNPs aggregation are found on the TEM grid, suggesting good dispersions of the nanoparticles in solution. DLS indicates the mean hydrodynamic radius of 94.4 nm (188.8 nm in diameters) with narrow size distribution, which agrees with the TEM images. The SAED pattern illustrates that the obtained PtNPs are single crystalline and adopt an fcc structure (Figure 11b, inset). The HR-TEM images shown in Figure 11b,c exhibit interplanar spacing of 0.23 nm, corresponding to the (111) planes fcc Pt. EDS (Figure S5a) and X-ray diffraction (Figure S5b) pattern confirm the nanoparticles are Pt (JCPDS No. 04-0802). Benefiting from the diversity of available similar precursor, such as chloroiridic acid and potassium hexachlororhodate, this approach is expected to be extended for preparation other metal nanoparticles. Moreover, it can be rationally envisioned that multiple compositional metal nanoparticles may be constructed when multiprecursor is employed in this synthetic strategy.

CONCLUSION

Facile synthesis of monodisperse water-soluble cholate-capped AuNPs with controllable sizes (13−70 nm) and narrow size distributions is realized by directly reducing hydrochloroauric acid with sodium cholate. The reaction process is conducted in aqueous solution at ambient temperature and is considered as a "green" process. The size and shape of as-obtained AuNPs can be tuned by changing cholate/$HAuCl_4$ ratio and solution pH. The obtained cholate-capped AuNPs exhibit a good electrocatalytic activity toward methanol oxidation, and the AuNPs thin films are found to serve as a useful substrate for surface-enhanced Raman scattering (SERS). Furthermore, platinum nanoparticles (PtNPs) can also be prepared through this method. The obtained uniform AuNPs and PtNPs functionalized by cholate molecules would find a wide range of biomedical applications owing to the biologically compatible characteristic.

ASSOCIATED CONTENT

Supporting Information. TEM images, DLS curves, UV−vis spectra, FT-IR spectra of AuNPs, and componential characterization of PtNPs. This material is available free of charge via the Internet at http://pubs.acs.org.

AUTHOR INFORMATION

Corresponding Author

*E-mail: jbhuang@pku.edu.cn; Fax: 86-10-62751708; Tel: 86-10-62753557.

ACKNOWLEDGMENT

This work was supported by National Natural Science Foundation of China (20873001, 50821061, and 21073006) and National Basic Research Program of China (Grant 2007CB936201). We thank Prof. Dr. Dongsheng Xu, Min Zhao, and Dr. Qin Xie for their help in electrocatalysis and SERS experiment.

REFERENCES

(1) Daniel, M. C.; Astruc, D. *Chem. Rev.* **2004**, *104*, 293–346.
(2) Jain, P. K.; Huang, X. H.; El-Sayed, I. H.; El-Sayed, M. A. *Acc. Chem. Res.* **2008**, *41*, 1578–1586.
(3) Hu, M.; Chen, J. Y.; Li, Z. Y.; Au, L.; Hartland, G. V.; Li, X. D.; Marquez, M.; Xia, Y. N. *Chem. Soc. Rev.* **2006**, *35*, 1084–1094.
(4) Wittstock, A.; Zielasek, V.; Biener, J.; Friend, C. M.; Baumer, M. *Science* **2010**, *327*, 319–322.
(5) Boisselier, E.; Astruc, D. *Chem. Soc. Rev.* **2009**, *38*, 1759–1782.
(6) Eustis, S.; El-Sayed, M. A. *Chem. Soc. Rev.* **2006**, *35*, 209–217.
(7) Murphy, C. J.; Gole, A. M.; Stone, J. W.; Sisco, P. N.; Alkilany, A. M.; Goldsmith, E. C.; Baxter, S. C. *Acc. Chem. Res.* **2008**, *41*, 1721–1730.
(8) Murphy, C. J.; Gole, A. M.; Hunyadi, S. E.; Stone, J. W.; Sisco, P. N.; Alkilany, A.; Kinard, B. E.; Hankins, P. *Chem. Commun.* **2008**, 544–557.
(9) Cobley, C. M.; Chen, J. Y.; Cho, E. C.; Wang, L. V.; Xia, Y. N. *Chem. Soc. Rev.* **2010**, *40*, 44–56.
(10) Ghosh, S. K.; Pal, T. *Chem. Rev.* **2007**, *107*, 4797–4862.
(11) Sperling, R. A.; Riveragil, P.; Zhang, F.; Zanella, M.; Parak, W. J. *Chem. Soc. Rev.* **2008**, *37*, 1896–1908.
(12) Sardar, R.; Funston, A. M.; Mulvaney, P.; Murray, R. W. *Langmuir* **2009**, *25*, 13840–13851.
(13) Wang, F.; Sun, L.-D.; Feng, W.; Chen, H. J.; Yeung, M. H.; Wang, J. F.; Yan, C.-H. *Small* **2010**, *6*, 2566–2575.
(14) Chen, H. J.; Shao, L.; Ming, T.; Sun, Z. H.; Zhao, C. M.; Yang, B. C.; Wang, J. F. *Small* **2010**, *6*, 2272–2280.
(15) Xu, R.; Sun, Y.; Yang, J.-Y.; He, L.; Nie, J.-C.; Li, L. L.; Li, Y. D. *Appl. Phys. Lett.* **2010**, *97*, 113101–113103.
(16) Liu, X. Q.; Niu, W. X.; Li, H. J.; Han, S.; Hu, L. Z.; Xu, G. B. *Electrochem. Commun.* **2008**, *10*, 1250–1253.
(17) Liao, H. G.; Jiang, Y. X.; Zhou, Z. Y.; Chen, S. P.; Sun, S. G. *Angew. Chem., Int. Ed.* **2008**, *47*, 9100–9103.
(18) Jin, R. C.; Cao, Y. C.; Hao, E. C.; Metraux, G. S.; Schatz, G. C.; Mirkin, C. A. *Nature* **2003**, *425*, 487–490.
(19) Niu, W. X.; Zheng, S. L.; Wang, D. W.; Liu, X. Q.; Li, H. J.; Han, S.; Chen, J.; Tang, Z. Y.; Xu, G. B. *J. Am. Chem. Soc.* **1996**, *131*, 697–703.
(20) Jin, R. C.; Cao, Y. C.; Hao, E. C.; Metraux, G. S.; Schatz, G. C.; Mirkin, C. A. *Nature* **2003**, *425*, 487–490.
(21) Alivisatos, A. P. *Science* **1996**, *271*, 933–937.
(22) Wang, X.; Zhuang, J.; Peng, Q.; Li, Y. D. *Nature* **2005**, *437*, 121–124.
(23) Bao, Z. H.; Sun, Z. H.; Li, Z. F.; Tian, L. W.; Ngai, T.; Wang, J. F. *Langmuir* **2011**, *27*, 5071–5075.
(24) Link, S.; El-Sayed, M. A. *J. Phys. Chem. B* **1999**, *103*, 8410–8426.
(25) Nehl, C. L.; Hafner, J. H. *J. Mater. Chem.* **2008**, *18*, 2415–2419.
(26) Murphy, C. J.; San, T. K.; Gole, A. M.; Orendorff, C. J.; Gao, J. X.; Gou, L.; Hunyadi, S. E.; Li, T. *J. Phys. Chem. B* **2005**, *109*, 13857–13870.
(27) Murphy, C. J.; Gole, A. M.; Hunyadi, S. E.; Orendorff, C. J. *Inorg. Chem.* **2006**, *45*, 7544–7554.
(28) Grzelczak, M.; Perez-Juste, J.; Mulvaney, P.; Liz-Marzan, L. M. *Chem. Soc. Rev.* **2008**, *37*, 1783–1791.

(29) Xia, Y.; Xiong, Y. J.; Lim, B.; Skrabalak, S. E. *Angew. Chem., Int. Ed.* **2009**, *48*, 60–103.
(30) Chen, J. Y.; Wiley, B. J.; Xia, Y. N. *Langmuir* **2007**, *23*, 4120–4129.
(31) Freeman, R. G.; Grabar, K. C.; Allison, K. J.; Bright, R. M.; Davis, J. A.; Guthrie, A. P.; Hommer, M. B.; Jackson, M. A.; Smith, P. C.; Walter, D. G.; Natan, M. J. *Science* **1995**, *267*, 1629–1632.
(32) Li, L. S.; Wang, Z. J.; Huang, T.; Xie, J. L.; Qi, L. M. *Langmuir* **2010**, *26*, 12330–12335.
(33) Ulman, A. *Chem. Rev.* **1996**, *96*, 1533–1554.
(34) Wang, R. Y.; Yang, J.; Zheng, Z. P.; Carducci, M. D.; Jiao, J.; Seraphin, S. *Angew. Chem., Int. Ed.* **2001**, *40*, 549–552.
(35) Petit, C.; Lixon, P.; Pileni, M. P. *J. Phys. Chem.* **1993**, *97*, 12974–12983.
(36) Suslick, K. S.; Fang, M. M.; Hyeon, T. *J. Am. Chem. Soc.* **1996**, *118*, 11960–11961.
(37) Weisbecker, C. S.; Merritt, M. V.; Whitesides, G. M. *Langmuir* **1996**, *12*, 3763–3772.
(38) Turkevich, J.; Stevenson, P. C.; Hillier, J. *Discuss. Faraday Soc.* **1951**, *11*, 55–75.
(39) Frens, G. *Nat. Phys. Sci.* **1973**, *241*, 20–22.
(40) Templeton, A. C.; Chen, S. W.; Gross, S. M.; Murray, R. W. *Langmuir* **1999**, *15*, 66–76.
(41) Gittins, D. I.; Caruso, F. *Angew. Chem., Int. Ed.* **2001**, *40*, 3001–3004.
(42) Wuelfing, W. P.; Gross, S. M.; Miles, D. T.; Murray, R. W. *J. Am. Chem. Soc.* **1998**, *120*, 12696–12697.
(43) Kanaras, A. G.; Kamounah, F. S.; Schaumburg, K.; Kiely, C. J.; Brust, M. *Chem. Commun.* **2002**, 2294–2295.
(44) Foos, E. E.; Snow, A. W.; Twigg, M. E.; Ancona, M. G. *Chem. Mater.* **2002**, *14*, 2401–2408.
(45) Hussain, I.; Graham, S.; Wang, Z. X.; Tan, B.; Sherrington, D. C.; Rannard, S. P.; Cooper, A. I.; Brust, M. *J. Am. Chem. Soc.* **2005**, *127*, 16398–16399.
(46) Wang, Z. X.; Tan, B. E.; Hussain, I.; Schaeffer, N.; Wyatt, M. F.; Brust, M.; Cooper, A. I. *Langmuir* **2007**, *23*, 885–895.
(47) Anastas, P. T.; Warner, J. C. *Green Chemistry: Theory and Practice*; Oxford University Press: New York, 1998.
(48) Matlack, A. S. *Introduction to Green Chemistry*; Marcel Dekker: New York, 2001.
(49) Dahl, J. A.; Maddux, B. L. S.; Hutchison, J. E. *Chem. Rev.* **2007**, *107*, 2228–2269.
(50) Poliakoff, M.; Anastas, P. *Nature* **2001**, *413*, 257–257.
(51) Murphy, C. J. *J. Mater. Chem.* **2008**, *18*, 2173–2176.
(52) DeSimone, J. M. *Science* **2002**, *297*, 799–803.
(53) Gross, R. A.; Kalra, B. *Science* **2002**, *297*, 803–807.
(54) Raveendran, P.; Fu, J.; Wallen, S. L. *J. Am. Chem. Soc.* **2003**, *125*, 13940–13941.
(55) Liu, J. C.; Qin, G. W.; Raveendran, P.; Kushima, Y. *Chem.—Eur. J.* **2006**, *12*, 2132–2138.
(56) Pande, S.; Ghosh, S. K.; Praharaj, S.; Panigrahi, S.; Basu, S.; Jana, S.; Pal, A.; Tsukuda, T.; Pal, T. *J. Phys. Chem. C* **2007**, *111*, 10806–10813.
(57) Qiao, Y.; Lin, Y. Y.; Wang, Y. J.; Yang, Z. Y.; Liu, J.; Zhou, J.; Yan, Y.; Huang, J. B. *Nano Lett.* **2009**, *9*, 4500–4504.
(58) Brown, W. *Dynamic Light Scattering: The Method and Some Applications*; Clarendon Press: Oxford, 1993.
(59) Berne, B. J.; Pecora, R. *Dynamic Light Scattering: With Applications to Chemistry, Biology, and Physics*; Dover Publications: Mineola, NY, 2000.
(60) Pons, T.; Uyeda, H. T.; Medintz, I. L.; Mattoussi, H. *J. Phys. Chem. B* **2006**, *110*, 20308–20316.
(61) Kannan, P.; John, S. A. *Nanotechnology* **2008**, 19.
(62) Wiley, B.; Sun, Y. G.; Chen, J. Y.; Cang, H.; Li, Z. Y.; Li, X. D.; Xia, Y. N. *MRS Bull.* **2005**, *30*, 356–361.
(63) Ji, X. H.; Song, X. N.; Li, J.; Bai, Y. B.; Yang, W. S.; Peng, X. G. *J. Am. Chem. Soc.* **2007**, *129*, 13939–13948.
(64) Kumar, S.; Gandhi, K. S.; Kumar, R. *Ind. Eng. Chem. Res.* **2007**, *46*, 3128–3136.
(65) Huang, T.; Meng, F.; Qi, L. M. *J. Phys. Chem. C* **2009**, *113*, 13636–13642.
(66) Maye, M. M.; Luo, J.; Lin, Y. H.; Engelhard, M. H.; Hepel, M.; Zhong, C. J. *Langmuir* **2003**, *19*, 125–131.
(67) Zhang, J. T.; Liu, P. P.; Ma, H. Y.; Ding, Y. *J. Phys. Chem. C* **2007**, *111*, 10382–10388.
(68) Zhong, C. J.; Maye, M. M. *Adv. Mater.* **2001**, *13*, 1507–1511.
(69) Borkowska, Z.; Tymosiak-Zielinska, A.; Shul, G. *Electrochim. Acta* **2004**, *49*, 1209–1220.
(70) Assiongbon, K. A.; Roy, D. *Surf. Sci.* **2005**, *594*, 99–119.
(71) Narayanan, R.; El-Sayed, M. A. *J. Phys. Chem. B* **2005**, *109*, 12663–12676.
(72) Jena, B. K.; Raj, C. R. *Langmuir* **2007**, *23*, 4064–4070.
(73) Jena, B. K.; Raj, C. R. *J. Phys. Chem. C* **2007**, *111*, 15146–15153.
(74) Trasatti, S.; Petrii, O. A. *Pure Appl. Chem.* **1991**, *63*, 711.
(75) Tremiliosi-Filho, G.; Gonzalez, E. R.; Motheo, A. J.; Belgsir, E. M.; Leger, J. M.; Lamy, C. *J. Electroanal. Chem.* **1998**, *444*, 31–39.
(76) Uetsuki, K.; Verma, P.; Yano, T.; Saito, Y.; Ichimura, T.; Kawata, S. *J. Phys. Chem. C* **2010**, *114*, 7515–7520.
(77) Huang, Y. F.; Zhu, H. P.; Liu, G. K.; Wu, D. Y.; Ren, B.; Tian, Z. Q. *J. Am. Chem. Soc.* **2010**, *132*, 9244–9246.
(78) Wang, T.; Hu, X. G.; Dong, S. J. *J. Phys. Chem. B* **2006**, *110*, 16930–16936.
(79) Wei, G.; Wang, L.; Liu, Z. G.; Song, Y. H.; Sun, L. L.; Yang, T.; Li, Z. A. *J. Phys. Chem. B* **2005**, *109*, 23941–23947.
(80) Fleischm., M.; Hendra, P. J.; McQuilla, A. J. *Chem. Phys. Lett.* **1974**, *26*, 163–166.
(81) Wang, T.; Zheng, R. B.; Hu, X. G.; Zhang, L. X.; Dong, S. J. *J. Phys. Chem. B* **2006**, *110*, 14179–14185.